

Catalytic Self-Assembled Monolayers on Au Nanoparticles: The Source of Catalysis of a Transphosphorylation Reaction

Giovanni Zaupa, Claudia Mora, Renato Bonomi, Leonard J. Prins,* and Paolo Scrimin*^[a]

Abstract: The catalytic activity of a series of Au monolayer protected colloids (Au MPCs) containing different ratios of the catalytic unit triazacyclononane-Zn^{II} (TACN·Zn^{II}) and an inert triethyleneglycol (TEG) unit was measured. The catalytic self-assembled monolayers (SAMs) are highly efficient in the transphosphorylation of 2-hydroxy propyl 4-nitrophenyl phosphate (HPNPP), an RNA model substrate, exhibiting maximum values for the Michaelis–Menten parameters k_{cat} and K_{M} of $6.7 \times 10^{-3} \text{ s}^{-1}$ and $3.1 \times 10^{-4} \text{ M}$, respectively, normalized per catalytic unit. Despite the structural simplicity of the catalytic units, this renders these nanoparticles among the most active catalysts known for this substrate. Both

k_{cat} and K_{M} parameters were determined as a function of the mole fraction of catalytic unit (x_1) in the SAM. Within this nanoparticle (NP) series, k_{cat} increases up till $x_1 \approx 0.4$, after which it remains constant and K_{M} decreases exponentially over the range studied. A theoretical analysis demonstrated that these trends are an intrinsic property of catalytic SAMs, in which catalysis originates from the cooperative effect between two neighboring catalytic units. The multivalency of the system

causes an increase of the number of potential dimeric catalytic sites composed of two catalytic units as a function of the x_1 , which causes an apparent increase in binding affinity (decrease in K_{M}). Simultaneously, the k_{cat} value is determined by the number of substrate molecules bound at saturation. For values of $x_1 > 0.4$, isolated catalytic units are no longer present and all catalytic units are involved in catalysis at saturation. Importantly, the observed trends are indicative of a random distribution of the thiols in the SAM. As indicated by the theoretical analysis, and confirmed by a control experiment, in case of clustering both k_{cat} and K_{M} values remain constant over the entire range of x_1 .

Keywords: gold • monolayers • nanoparticles • self-assembly • supported catalysts • transphosphorylation

Introduction

The increasing demand for highly atom-efficient chemical transformations with a low environmental impact makes the development of new catalysts one of the crucial challenges for chemists.^[1] Traditionally, catalysts are classified as either homogeneous or heterogeneous depending whether the catalyst is solubilized in the reaction medium or supported on a solid phase. The main advantage of homogeneous catalysts is that specificity, activity, and selectivity is determined by their molecular architecture, which allows these properties to be tuned in a rational fashion. On the other hand, the recovery and re-use of homogeneous catalysts is complicated, and for that reason large industrial processes rely for a large part on heterogeneous catalysts. A current trend in catalyst design is the development of hybrid systems that combine

the advantages of homogeneous and heterogeneous catalysts.^[2] Examples include the incorporation of molecular complexes, or clusters on surfaces or in pores of otherwise inert supports, such as silica,^[3,4] clays,^[5] zeolites,^[6] and resins.^[7] In most cases, the inert support serves only to facilitate catalyst recovery. A next step towards catalytic architectures are those systems in which the support also plays an additive role in the catalytic performance. An example are the so-called metal complex@metal systems obtained by immobilization of an organometallic complex on a metal nanoparticle.^[8] A second example are self-assembled monolayers (SAMs) of catalysts on inorganic nanoparticles.^[9–11] Here, the nanoparticle serves as a large structural unit on which multiple catalytic complexes are assembled. Also here, the inorganic core allows recovery of the catalytic system through filtration,^[12] or magnetic separation,^[13,14] but the advantages go far beyond that. As illustrated by us^[15–17] and others,^[18] the multivalent nature of Au nanoparticles can give rise to cooperative effects between catalytic units. In the past, similar effects have also been observed in micelles and vesicles, but the much lower stability of these aggregates poses limits to their application and in most cases does not permit catalysis under turnover conditions.^[19–21] A related class of multivalent platforms are dendrimers, which have gained an enormous interest, amongst others for their ability

[a] Dr. G. Zaupa, C. Mora, Dr. R. Bonomi, Dr. L. J. Prins, Prof. Dr. P. Scrimin
Department of Chemical Sciences and CNR-ITM
Padova Section, Via Marzolo 1, 35131 Padova, (Italy)
Fax: (+39) 0498275239
E-mail: leonard.prins@unipd.it
paolo.scrimin@unipd.it

Supporting information for this article is available on the WWW under <http://dx.doi.org/10.1002/chem.201002590>.

to induce cooperative effects between peripheral catalytic units.^[22] In fact, the term “dendritic effect” describes the increase in dendrimer performance as a function of its valency.^[23–26] Compared to Au monolayer protected colloids (Au MPCs), however, their synthesis and purification is much more cumbersome.

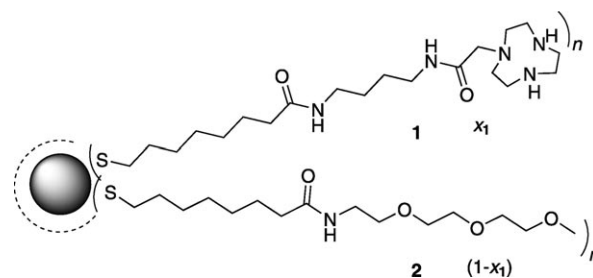
Recently, it has been shown that in mixed monolayers on Au NPs the properties of the catalytic units may be steered by the surrounding inert units.^[27] This opens up the exciting perspective of modulating the catalytic properties of the system simply by changing the composition of the monolayer. Clearly, in such a system the overall catalytic performance is strongly determined by the structural order of the SAM, that is, the orientation of the catalytic complexes with respect to each other or other functionalities. Recently, observations indicating the formation of homodomains or clusters in mixed SAMs have been reported.^[28–30] Evidently, from the perspective of controlling the properties of catalysts within a mixed monolayer, it is of crucial importance to know the structural order of the SAM.^[31] However, studies that correlate the catalytic performance to the composition of the SAM are hitherto nearly absent.^[11] Here, we perform such an in-depth study on a catalytic Au-NP-based system that we had already earlier shown to be highly efficient in catalyzing the transphosphorylation of 2-hydroxypropyl 4-nitrophenyl phosphate (HPNPP), an RNA model substrate.^[15] The study of a series of Au MPCs with various catalyst loadings on the surface gives for the first time a correlation between catalyst loading and overall catalytic efficiency. We address the important question whether the catalytic sites, once formed, change upon increasing the mole fraction of catalytic units and whether “dendritic effects” occur. In addition, it is shown that the obtained correlation can be used to gain information on the structural order within mixed SAMs as well as on the source of catalysis in these systems.

Results and Discussion

The synthetic protocol for the preparation of mixed thiol monolayers on Au NPs follows a modified literature procedure^[32] originally developed by Jana and Peng.^[33] This protocol relies on the initial formation of Au NPs transiently stabilized with secondary amines (a synthetic scheme is given in the Supporting Information). Here, the ratio of dioctylamine:HAuCl₄ determines the size of the Au NPs, which can range from 1.5–7.0 nm.^[32] In a subsequent step the dioctylamines are replaced under mild conditions with the desired thiols to give the final products. This two-step protocol offers an important advantage over other synthetic protocols. Only the minimal amount of thiol necessary to cover the Au NPs needs to be added, which means that an excess of thiol is hardly present. Accordingly, the composition of mixed monolayers neatly reflects the composition of the mixture of thiols added. Compared to other methods based on thiol exchange,^[34–37] this gives a much larger control over

the monolayer composition and it has been shown that this allows virtually all ratios of thiols in a binary mixture to be addressed.^[32,38]

In this work, we prepared mixed SAMs composed of thiol **1**,^[32] containing a triazacyclononane (TACN) head group that forms a stable complex with Zn^{II}-ions, and thiol **2**,^[39] containing a TEG head group that renders the NPs soluble in aqueous solution (Scheme 1). Previously, we have shown



Scheme 1. Au MPCs functionalized with thiols **1** and **2**.

that multivalent systems, such as tripodal ligands,^[40] dendrimers,^[41–43] and Au NPs,^[15] that contain multiple copies of the TACN·Zn^{II}-complex are highly efficient catalysts for the transphosphorylation of HPNPP. For all systems, kinetic Zn^{II} titrations revealed that catalysis requires the cooperative action of two TACN·Zn^{II} complexes. The isolated TACN·Zn^{II} complex is practically inactive in catalyzing this reaction.^[15] This feature makes this catalytic system intrinsically very well-suited to be implemented in multivalent systems, similar to imidazoles for ester hydrolysis^[26,44,45] or the Jacobsen salen complexes (salen = *N,N'*-ethylenebis(salicylimine)) for asymmetric epoxidation reactions.^[46] Compared to our previous studies,^[15] we have modified the TACN-functionalized thiol, eliminating the terminal amide group. This modification facilitated the synthesis and also had some beneficial effect on the catalytic activity.

To study the correlation between surface coverage and catalytic activity we prepared a series of Au NPs (**I–VII**) protected with thiols **1** and **2** in the ratios indicated in Table 1. To ensure an identical core size for all Au NPs the

Table 1. Monolayer composition of Au MPCs **I–VIII** determined by ¹H NMR spectroscopy (LEDbp and after I₂ oxidation) and UV/Vis spectroscopy.

NP batch	Expected	x_1 ^[a]		UV/Vis Cu ^{II}	av ^[b]
		NMR LEDbp	NMR after I ₂		
I	1.00	–	–	–	1.00
II	0.80	0.79	0.72	0.72	0.74
III	0.60	0.60	0.54	0.56	0.56
IV	0.40	0.40	0.34	0.31	0.35
V	0.20	0.15	0.15	0.20	0.17
VI	0.10	0.09	N.D. ^[c]	0.11	0.10
VII	0.05	0.04	N.D.	0.06	0.05
VIII	0	–	–	–	0

[a] x_1 is the mole fraction of **1** on the NP surface. [b] We estimate the final error in the x_1 values to be <0.05. [c] N.D. = not determined.

initial batch of dioctylamine-stabilized Au NPs was split into eight batches to which thiols **1** and **2** were added in the desired ratios. All nanoparticle batches were completely soluble in water. Before assessing their catalytic activity, a variety of analytical techniques was used to characterize the Au MPCs and to determine the obtained ratio of thiols **1** and **2** in the monolayer.

Size of the Au core: The diameter of the gold nuclei was determined as 1.6 ± 0.2 nm by means of HR-TEM (for a representative example see Figure 1). The absence of the surface plasmon resonance band at 520 nm in the UV/Vis spectrum gave additional proof for the presence of sub 2 nm sized NPs and, importantly, for the absence of clustered gold nanoparticles (Figure 1c).

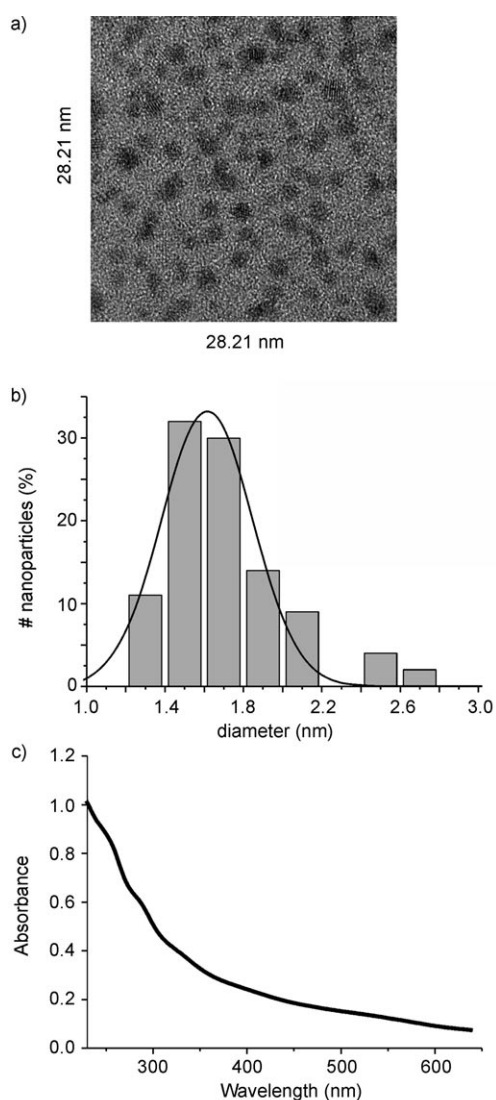


Figure 1. a) Representative example of a HR-TEM image (sample **I**). b) Size distribution of the Au NPs. c) Representative UV/Vis spectrum indicating the absence of the surface plasmon band at 520 nm.

Monolayer composition: Of fundamental importance in this study is the composition of the monolayer in terms of the thiol ratio **1:2**. This parameter was assessed in a variety of ways. Diffusion-ordered ^1H NMR spectra were recorded using the low eddy currents distortion bipolar gradients (LEDbp) sequence,^[47] which allows differentiation of molecules based on their diffusion coefficients.^[48] Not only does this provide unequivocal confirmation that the thiols are bound to the Au NP surface, but also provides a way to assess the purity of the samples. The obtained NMR spectra with and without the diffusion filter showed that only minimal amounts of unbound additives were present in the purified samples (see Supporting Information; for an example, see Figure 2a and 2b). For each batch, the thiol ratio **1:2** was determined by integration of characteristic signals for each of the thiols (**1**: $\delta = 2.9$ ppm; **2**: $\delta = 3.4\text{--}3.6$ ppm) calibrated on a reference signal common to both thiols ($\delta = 2.13$ ppm) (for a representative example, see Figure 2c). To verify that integration of the broad signals did not cause large errors, all integrations were repeated after treatment of the Au MPCs with I_2 . Addition of I_2 causes a decomposition of the Au MPCs and the formation of disulfides (both homomeric and heteromeric). No longer being adsorbed on the nanoparticle, the ^1H NMR spectra of the organic compounds exhibit sharp signals which can be readily integrated (see Supporting Information). The **1:2** ratios thus determined did not substantially differentiate from those previously determined.

The concentration of TACN head groups was also determined by means of a spectrophotometric titration of each batch of nanoparticles with Cu^{II} , taking advantage of the characteristic absorbance of the 1:1 TACN: Cu^{II} complex at 264 nm ($\epsilon_{264} = 7800 \text{ L mol}^{-1} \text{ cm}^{-1}$ compared to $800 \text{ L mol}^{-1} \text{ cm}^{-1}$ for free Cu^{II}). The result of one such a titration is given in Figure 3 (for details see the Experimental Section). The absorbance increases linearly up till a saturation of all TACN ligands with Cu^{II} . The slight increase in absorbance after the addition of one equivalent of Cu^{II} corresponds to free Cu^{II} in solution. The obtained concentrations of TACN were found to be in good agreement with those obtained from the ^1H NMR studies. Finally, kinetic titrations using Zn^{II} (see next paragraph) gave additional proof for the monolayer composition.

Catalytic activity: The catalytic activity of Au MPCs **I–VII** (TEG-functionalized Au MPC **VIII** is not catalytically active) in the transesterification of HPNPP^[49] was first evaluated by means of kinetic titrations with Zn^{II} . In these experiments the amount of Zn^{II} is gradually increased at constant Au MPC concentration and the initial rate is determined by measuring the amount of released *p*-nitrophenolate ion in time (Scheme 2). It should be noted that all kinetic studies that will be described in this work were performed at the same nominal concentration of TACN ($20 \mu\text{M}$). This allows for a direct comparison of the catalytic activity of each NP batch, since numerical contributions are eliminated. Evidently, this implies that the concentration of

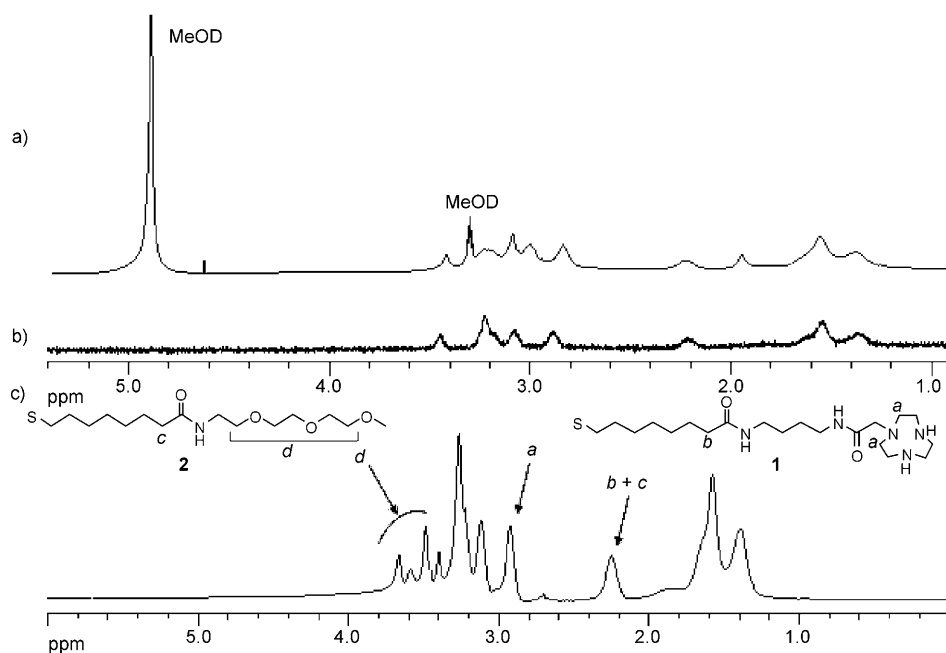


Figure 2. a) Part of the ^1H NMR spectrum of NP batch I. b) The same sample using the LEDbp sequence. c) Part of the ^1H NMR spectrum of NP batch II indicating the signals used for quantification. All spectra are recorded in $[\text{D}_2]\text{MeOD}$ (300 MHz, 301 K).

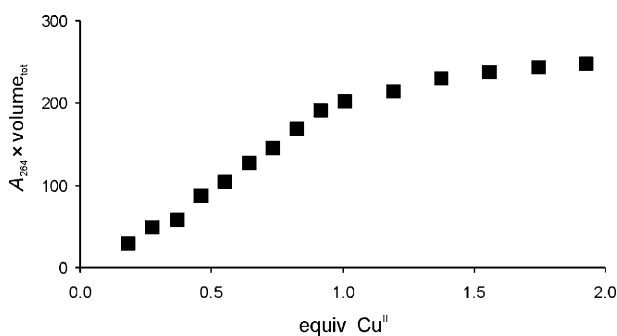
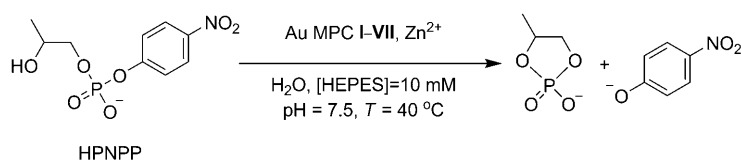


Figure 3. Changes in the absorbance at 264 nm of Au NP batch I upon the addition of Cu^{II} . For a detailed description see the Experimental Section.



Scheme 2. Transphosphorylation of HPNPP.

NPs increases as the surface loading decreases. Potentially this might affect the catalytic parameters, which is an issue that will be addressed separately. Plots of the initial rates against the amount of added Zn^{II} already provide much information on the behavior of these systems, which bear much resemblance to the TACN-based systems that we have studied earlier (Figure 4a).^[15,41] First, the pivotal role of Zn^{II} is evident from the absence of catalytic activity for the NPs

without Zn^{II} . Second, the catalytic activity continues to increase until TACN and Zn^{II} are present in a 1:1 ratio, indicating that the TACN· Zn^{II} complex is the catalytic unit. Additionally, this also provides final evidence that the TACN surface loadings as determined in the previous paragraph are correct. Third, analogous to previously studied multivalent systems,^[15,41] sigmoidal curves are obtained indicating that the process is cooperative and the catalytic site is composed of two TACN· Zn^{II} complexes.^[50] Finally, a simple glance on the curves tells immediately that the catalytic activity strongly increases as a function of the surface loading of TACN.

Subsequently, the catalytic performances of each nanoparticle batch I–VII were assessed separately (in the presence of

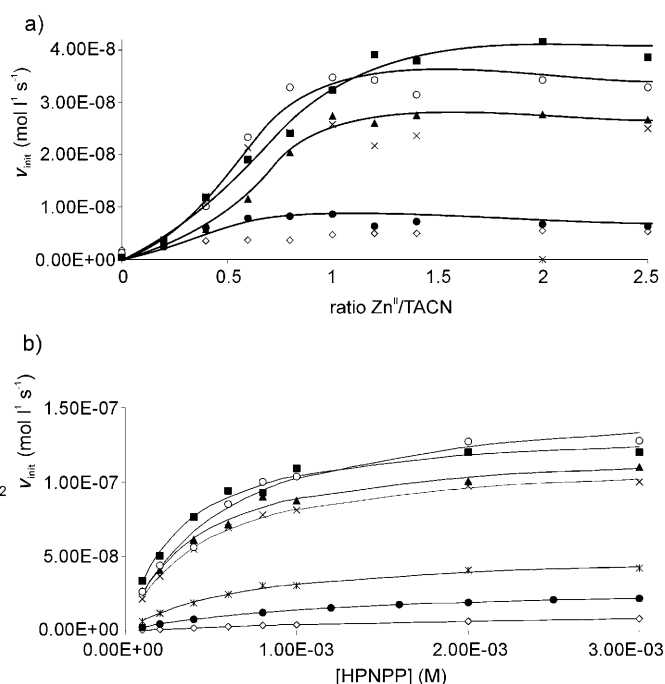


Figure 4. a) Initial rates for the cleavage of HPNPP by NP batch I (■), II (○), III (▲), IV (×), VI (●), and VII (◇) as a function of the equivalents of Zn^{II} added. Conditions: $[\text{TACN}] = 2 \times 10^{-5} \text{ M}$, $[\text{HPNPP}] = 2 \times 10^{-4} \text{ M}$, $[\text{HEPES}] = 1 \times 10^{-2} \text{ M}$, pH 7.5, $T = 40^\circ\text{C}$. For 4 batches trendlines are added to indicate the sigmoidal behavior. b) Initial rates for the cleavage of HPNPP by NP batch I (■), II (○), III (▲), IV (×), V (*), VI (●), and VII (◇) as a function of the substrate concentration. Conditions: $[\text{TACN}] = 2 \times 10^{-5} \text{ M}$, $[\text{Zn}(\text{NO}_3)_2] = 2 \times 10^{-5} \text{ M}$, $[\text{HEPES}] = 1 \times 10^{-2} \text{ M}$, pH 7.5, $T = 40^\circ\text{C}$. Solid lines indicate the best fits to the Michaelis–Menten equation. Errors are typically $\leq 10\%$.

one equivalent of Zn^{II} per TACN) by measuring the initial reaction rates in the presence of increasing amounts of substrate HPNPP, that is, under turn-over conditions (experiment series **A**, Figure 4b). Enzyme-like saturation curves were obtained, which were fitted to the Michaelis–Menten equation $v_{\text{init}} = k_{\text{cat}}[\text{TACN}\cdot\text{Zn}^{\text{II}}][\text{S}]/(K_{\text{M}} + [\text{S}])$ yielding the Michaelis–Menten parameters k_{cat} and K_{M} for each nanoparticle batch **I–VII**.

In experiment series **B**, increasing amounts of TEG-functionalized nanoparticles **VIII** were mixed with a constant amount of nanoparticles **I** (and one equivalent of Zn^{II} per TACN). Thus, in this series exclusively homofunctionalized nanoparticles (containing either TACN- or TEG-head groups) were used.^[51] For each ratio **I:VIII** the Michaelis–Menten parameters were obtained from the respective saturation profiles. The resulting Michaelis–Menten parameters for both experiment series **A** and **B** are given in Tables 2 and 3 and plotted in Figure 5 as a function of the mole frac-

Table 2. Michaelis–Menten parameters for Au MPCs I–VII (experiment series **A**). Parameters for multivalent systems **3–5** are added for comparison. These last values are normalized for the number of Zn^{II} ions present.

System	k_{cat} [$\times 10^{-3} \text{ s}^{-1}$]	K_{M} [$\times 10^{-3} \text{ M}$]	$k_{\text{cat}}/K_{\text{M}}$ [$\text{L mol}^{-1} \text{ s}^{-1}$]	$k_{\text{cat}}/k_{\text{uncat}}^{\text{[b]}}$
I ^[a]	6.7 ± 0.6	0.3 ± 0.1	21.7 ± 4.7	33 587
II ^[a]	7.9 ± 0.8	0.5 ± 0.1	14.8 ± 2.9	39 313
III ^[a]	6.1 ± 0.6	0.4 ± 0.1	15.8 ± 3.1	30 529
IV ^[a]	5.9 ± 0.6	0.4 ± 0.1	13.7 ± 2.7	29 327
V ^[a]	2.6 ± 0.3	0.7 ± 0.1	3.8 ± 0.8	13 095
VI ^[a]	1.5 ± 0.2	1.2 ± 0.1	1.2 ± 0.3	7 586
VII ^[a]	0.8 ± 0.1	2.8 ± 0.4	0.3 ± 0.1	3 842
3 ^[e,f]	0.6	1.2	0.5	3 000
4 ^[d,f]	0.1	3.9	0.03	500
5 ^[e,f]	8.5	0.32	26.6	42 500

[a] Conditions as given in the legend of Figure 5. [b] $k_{\text{uncat}} = 2 \times 10^{-7} \text{ s}^{-1}$. [c] Taken from reference [42]. [d] Taken from reference [58]. [e] Taken from reference [52]. [f] The structures of **3**, **4** and **5** are given in Figure 8.

Table 3. Michaelis–Menten parameters for mixtures of Au MPCs **I** and **VIII** in different ratios (experiment series **B**).

Ratio I/VIII	k_{cat} [$\times 10^{-3} \text{ s}^{-1}$]	K_{M} [$\times 10^{-3} \text{ M}$]	$k_{\text{cat}}/K_{\text{M}}$ [$\text{L mol}^{-1} \text{ s}^{-1}$]
1.00	6.7 ± 0.6	0.3 ± 0.1	21.7 ± 4.7
0.50	5.0 ± 0.6	0.3 ± 0.1	17.6 ± 4.6
0.17	5.7 ± 0.6	0.3 ± 0.1	17.3 ± 3.9
0.09	4.8 ± 0.5	0.4 ± 0.1	13.0 ± 2.4

[a] Conditions as given in the legend of Figure 5. [b] $k_{\text{uncat}} = 2 \times 10^{-7} \text{ s}^{-1}$.

tion x_1 . The graphs will be discussed extensively in the final section of this manuscript, but at first glance immediately some trends can be evidenced. First, nanoparticles with a high surface loading of catalyst ($x_1 > 0.5$) are characterized by a high catalytic activity ($k_{\text{cat}}/k_{\text{uncat}} > 30\,000$) and high affinity for the substrate (K_{M} in the sub- μM range), which combine to give a $k_{\text{cat}}/K_{\text{M}}$ value of $21.7 \text{ L mol}^{-1} \text{ s}^{-1}$ for $x_1 = 1$. This makes this system among the most potent catalysts reported for this reaction (the best-performing dinuclear catalyst **5**^[52] is added as a comparison in Table 2; for a detailed

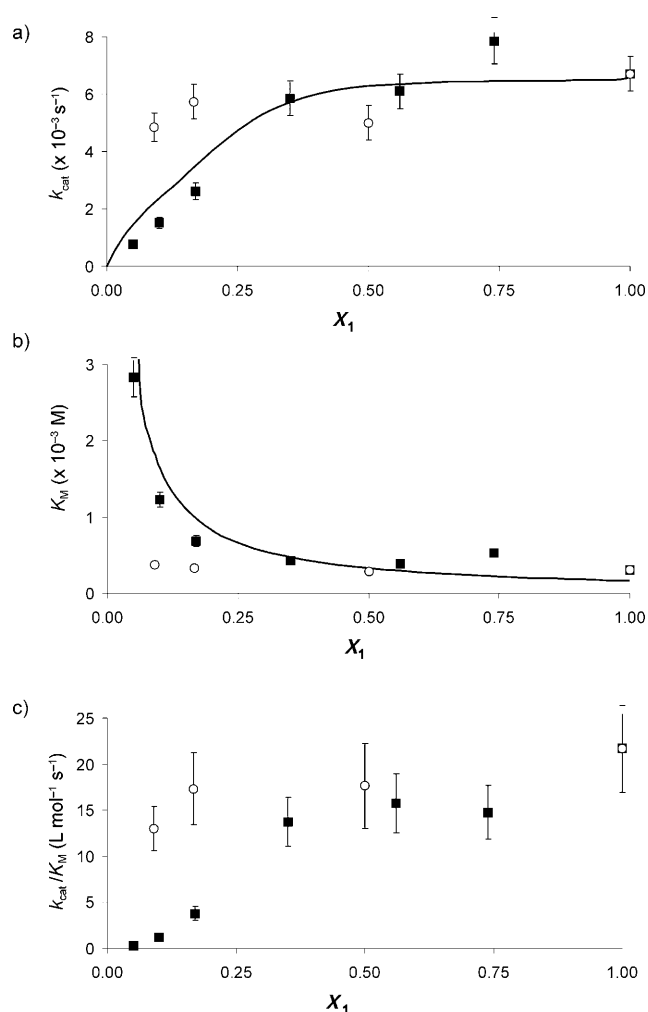


Figure 5. Experimentally obtained Michaelis–Menten parameters a) k_{cat} , b) K_{M} , and c) $k_{\text{cat}}/K_{\text{M}}$ as a function of x_1 for experiment series **A** (■) and **B** (○). The solid lines in a) and b) are the calculated values for randomly distributed thiols in the SAM according to the model (see Figure 7).

list of catalysts see references [53,54]). It has previously been shown that the single TACN· Zn^{II} complex is a very poor catalyst, exhibiting an apparent second-order rate constant of $0.007 \text{ M}^{-1} \text{ s}^{-1}$ (pH 7.4, 40°C).^[15] Second, for series **A** and **B** a different correlation is observed between the parameters k_{cat} and K_{M} and the mole fraction x_1 (Figure 5a,b). For series **B** both parameters are nearly constant over the range of mole fractions studied. For series **A**, however, k_{cat} increases in a linear manner up till $x_1 \approx 0.4$ after which it levels off. K_{M} shows an exponential decay, indicative of a significant increase in substrate affinity as the catalyst surface loading increases. The combined positive effects of k_{cat} and K_{M} result in an almost linear increase of the second-order rate constant $k_{\text{cat}}/K_{\text{M}}$ as a function of x_1 . In terms of the second-order rate constant, the single TACN· Zn^{II} complex is almost 80-fold more active in batch **I** ($x_1 = 1$) compared to batch **VII** ($x_1 = 0.05$). For series **B** the difference is negligible (1.5-fold). This is strongly indicative of a positive dendritic effect, similar to that observed in den-

drimers. However, before interpreting these correlations it is important to first analyze which kind of trends in k_{cat} and K_{M} are expressed intrinsically by this kind of multivalent systems.

Theoretical analysis: Enzyme-like behavior of a catalyst implies the occurrence of an initial binding event between the catalyst and the substrate, characterized by a dissociation constant K_{M} , followed by the conversion of substrate into product, characterized by a first-order rate constant k_{cat} . The consequence is a saturation profile when the initial rate of reaction (v_{init}) is plotted as a function of substrate concentration, $[S]$. This graph is defined by a second-order regime at low substrate concentration ($[S] \ll K_{\text{M}}$ for which $v_{\text{init}} = (k_{\text{cat}}/K_{\text{M}})[E][S]$; $[E]$ = “enzyme” or catalyst concentration) and a first-order regime at high substrate concentrations ($[S] \gg K_{\text{M}}$ for which $v_{\text{init}} = k_{\text{cat}}[E]$). The Michaelis–Menten equation is designed to describe the behavior of a single substrate–enzyme interaction. The interpretation of the Michaelis–Menten parameters for multivalent enzyme-like catalysts is not straightforward, because in such systems multiple substrate–enzyme interactions take place simultaneously. The experimentally obtained values are therefore average values of all single binding and catalytic events. To have a meaningful discussion of these “averaged” values, one has to know the intrinsic effect originating from the multivalency of the system. Previously we have performed such an analysis on a series of homofunctionalised dendrimers of increasing valency.^[42] Rather interestingly, we observed that the clustering of catalytic units on a multivalent scaffold gives spontaneously rise to a positive dendritic effect; that is, an increased catalytic efficiency ($k_{\text{cat}}/K_{\text{M}}$) as a function of the dendrimer valency on the condition that catalysis requires the simultaneous action of two catalytic units. A theoretical analysis showed that this intrinsic dendritic effect originates from the fact that the concentration of catalytic sites (composed of two units) increases more than linearly as a function of the valency of the system. In other words, the same number of catalytic units can create more catalytic sites in case the valency is higher. Consequently, the “apparent” concentration of catalytic sites is much higher than the nominal concentration of catalytic units. This implies that fitting of the saturation profile using the classical Michaelis–Menten equation (taking the concentration of catalytic units as reference) yields an “overall” value for K_{M} that decreases as a function of the valency (suggesting stronger binding). This decrease in the “overall” K_{M} value is an intrinsic property of multivalent systems and has nothing to do with the actual binding affinity between the catalytic site and the substrate (which remains constant). Additionally, we showed that the catalytic efficiency of the multivalent system at saturation (where $v_{\text{init}} = k_{\text{cat}}[E]$) is determined by the actual number of catalytic units that are participating in the formation of catalytic sites. The “overall” k_{cat} value is lowered by the presence of isolated catalytic units unable to form a dimeric catalytic site. Furthermore, an alteration of the catalytic site as a function of valency (distance between the catalytic units, polarity,

local pH, etc.) will additionally affect the “overall” Michaelis–Menten parameters (either positively or negatively). To correctly interpret the data of the NP-based systems presented in this study we need first to establish the intrinsic changes of the “overall” Michaelis–Menten parameters, K_{M} and k_{cat} , as a function of the composition of the mixed monolayers. It is evident that these changes will also depend on the structural order of the monolayer, that is, whether the two thiols **1** (catalytic unit) and **2** (inert unit) are randomly distributed or present in clusters or homodomains. These boundary conditions will both be addressed. To evaluate the correlation between K_{M} , k_{cat} , and the mole fraction x_1 on the surface, we took a truncated icosahedron as a simple model for a spherical nanoparticle.^[55] A truncated icosahedron is an Archimedean solid composed of 12 pentagonal and 20 hexagonal faces. It was assumed that each face can accommodate one unit of **1** or **2**. This implies that at full surface coverage 32 units are bound. In this model each unit has five or six neighboring units, which corresponds reasonably to the packing of SAMs of thiols on Au surfaces. The only catalytically relevant species is the dimeric site **1–1** formed between two neighboring units **1**. In all simulations the **1–1** site has constant K_{M} and k_{cat} values. Contributions from the single catalytic unit **1** and the dimeric site **1–2** to catalysis were not included.

A statistical distribution of units of **1** on the surface was simulated by the stepwise random insertion of **1** on the facets of the model completely covered with **2** ($x_1 = 0$). This was repeated until all facets were occupied with **1** ($x_1 = 1$). After each addition, the number of catalytic dimeric sites **1–1** was counted and also the number of dimeric sites **1–1** that could be occupied simultaneously. It is evident that the first number is higher than the second, because a single catalytic unit **1** can potentially form a catalytic site with each of its **1** neighbors, but effectively can participate in the binding of one substrate molecule only. This is exemplified in Figure 6a, which depicts the number of potential catalytic sites and the effective catalytic sites for $x_1 = 0.5$. Assuming that for a given amount of **1** and **2** SAMs are formed according to a binomial distribution and normalizing for the amount of **1** present (meaning that the concentration of **1** is a constant) gives the profiles for the number of initial binding sites and for the maximum number of substrate molecules bound as a function of the mole fraction x_1 as depicted in Figure 7 (■). Next, homodomain formation of **1** was simulated by inserting new **1** units on the facets of the model on positions neighboring other **1** units (Figure 6b). Also here, it was assumed that SAMs are formed according to a binomial distribution of **1** and **2** on different nanoparticles. This assumption implies that clustering occurs after monolayer formation. The resulting profiles are also depicted in Figure 7 (□). Clustering during monolayer formation effectively means the tendency of the thiols to self-sort preferentially on different nanoparticles, which in an extreme case means that only homomeric **1** and **2** nanoparticles are present. Normalized on the concentration of **1** would give constant K_{M} and k_{cat} values independent of x_1 . This situation is added to

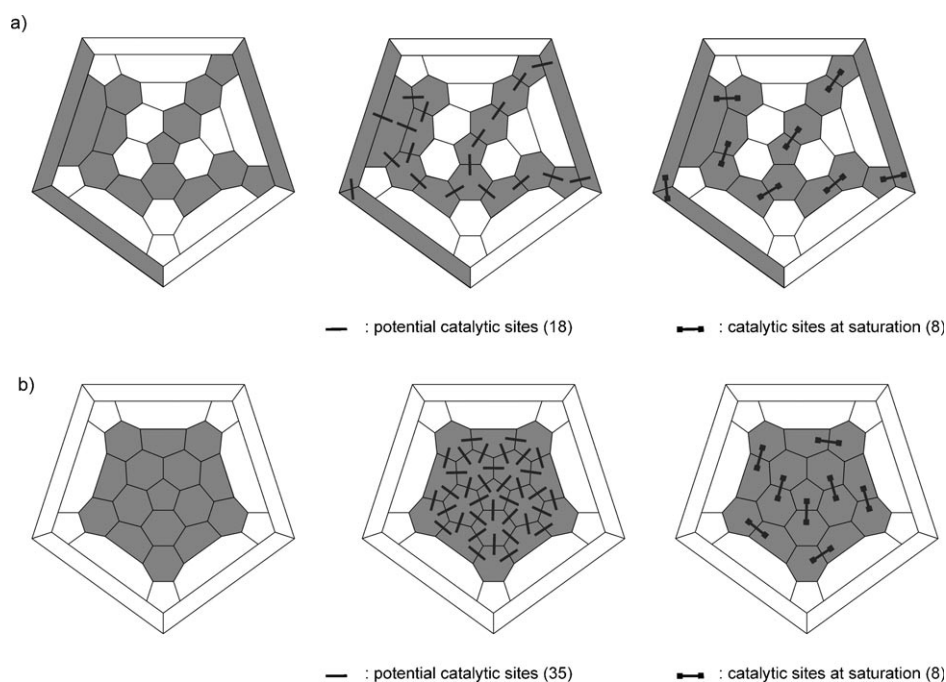


Figure 6. Simulation of catalytic units **1** (grey areas) on a truncated icosahedron for $x_1=0.5$: a) random distribution or b) homodomain formation. Solid lines indicate potential catalytic sites (dimers **1-1**) for the first substrate. Solid lines terminated with dots indicate catalytic sites at saturation.

Figure 7 (○) and represents an extreme case of clustering. Together, both profiles represent the boundaries for clustering.

The dissociation constant K_M : In case of a statistical distribution of **1**, the concentration of dimeric sites **1-1** increases strictly linearly as a function of the mole fraction x_1 . This implies that the same number of units of **1** is able to generate more potential catalytic sites **1-1** as the surface loading increases. If **1** has a tendency to cluster, the amount of catalytic sites on the surface is much less dependent on the mole fraction x_1 . The concentration of **1-1** rapidly increases up to $x_1 \approx 0.2$, after which it slowly increases to the final value. The lower concentration of **1-1** compared to the homomeric SAMs ($x_1=1$) results from units of **1** localized on the border of the clusters. In fact, clustering resulting from self-sorting during monolayer formation results in a concentration of **1-1** independent from x_1 . In all cases, the higher apparent concentration of catalytic sites will result in an apparent increase in binding affinity (lower K_M values). The anticipated correlation between K_M and mole fraction x_1 for the three situations is given in Figure 7b (which is the inverse of the concentration of [**1-1**] normalized on **1** for $x_1=1$).

The catalytic constant k_{cat} : The number of substrate molecules bound at saturation is directly correlated to k_{cat} . For a random distribution of **1**, k_{cat} reaches a maximum at $x_1 \approx 0.4$ (Figure 7c). Thus, k_{cat} does not increase linearly with x_1 as would be expected in a non-confined environment. This situation is different from that reported by Regen when con-

sidering the nearest-neighbor recognition in vesicular aggregates.^[56,57] This difference arises from the fact that, contrary to Regen's system, here the heterodimeric site **1-2** cannot bind a substrate molecule. At lower surface loadings, isolated catalytic units **1** are present, which are unable to participate in the formation of a catalytic site **1-1**. Evidently, in the case of cluster formation, isolated units of **1** are never present and a maximum value for k_{cat} is already reached at $x_1 \approx 0.15$ (Figure 7c). Below this value, decreased k_{cat} values result from the presence of small clusters with an odd number of units **1** (e.g., 3 or 5), which implies that at saturation some units do not participate in catalysis.

Summarizing, Figure 7b and 7c are indicative of the intrinsic behavior of catalytic SAMs with regard to the apparent Michaelis–Menten parameters k_{cat} and K_M and form the reference framework against which to analyze the experimental data. This implies that identical experimental profiles do not require any chemical explanation, but can be attributed merely to statistics. Alternatively, a deviation from the anticipated intrinsic behavior implies that the Michaelis–Menten parameters k_{cat} and K_M for the individual catalytic sites are not constant. This indicates a change in the catalytic site or local environment as a function of the surface coverage.

Analysis of the experimental data: Experimentally we have varied the mole fraction of the catalytic unit TACN·Zn^{II} (x_1) in the system in two different ways. In experiment series **A**, Au MPCs were prepared with mixed monolayers composed of thiols **1** and **2** in various ratios. In series **B**, increasing amounts of TEG-functionalized nanoparticle **VIII** were added to a constant amount of TACN-functionalized nanoparticle **I** in the presence of one equivalent of Zn^{II} per TACN. We were interested in the following key questions:

1) Are the experimentally observed correlations between the k_{cat} and K_M values in the mixed monolayer system an intrinsic consequence of the multivalency of the system or can they be ascribed to a “true” dendritic effect (implying actual improvements in the catalytic site)?

2) Do the correlations provide information on the structural order of the mixed monolayers in terms of clustering or statistical distribution?

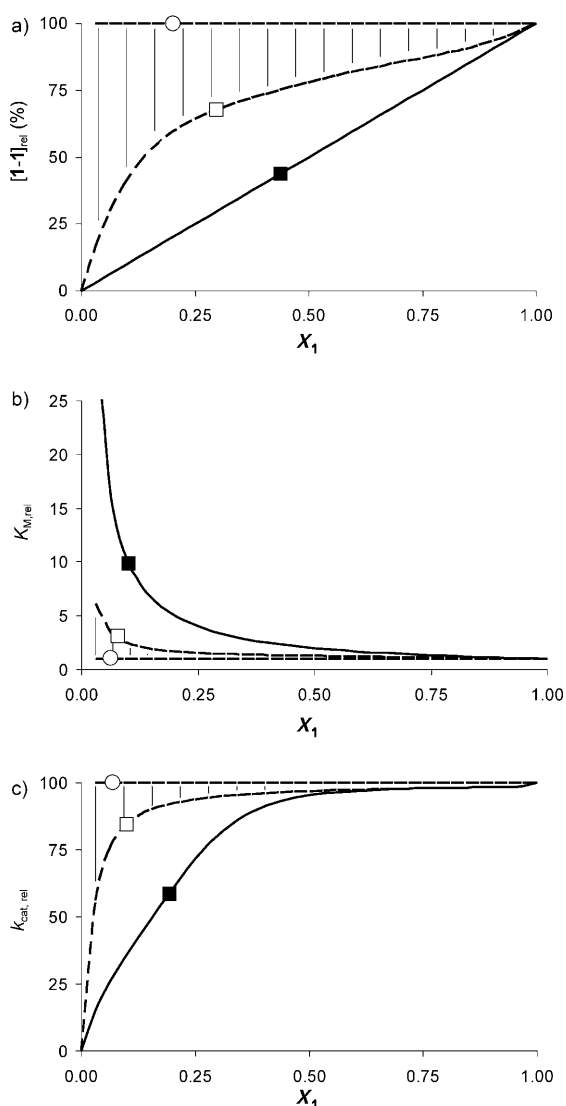


Figure 7. Simulated correlations between a) the concentration of dimeric sites **1-1**, b) K_M and c) k_{cat} as a function of the mole fraction x_1 . The solid line marked with (■) represents the correlation in case **1** is randomly distributed on the surface. The dashed line marked with (□) represent homodomain formation of **1** after monolayer formation. The dashed line marked with (○) represent self-sorting of thiols on different nanoparticles during monolayer formation.

3) What is the origin of the much higher catalytic activity of these nanoparticles compared to related multivalent systems based on the identical TACN·Zn^{II} complex?

The results of experiment series **B** represent what would be observed in case the two thiols **1** and **2** would perfectly separate in two phases on the nanoparticle surface, that is, addition of the two thiols to the amine-stabilized nanoparticles results in the formation of exclusively homofunctionalized nanoparticles. From the observed trend for this series it appears that the catalytic properties, both in terms of k_{cat} and K_M , of the catalytic unit TACN·Zn^{II} are rather unaffected by the presence of the inert thiol **2** (Figure 5:○). This corresponds to the expectation based on intuition, and also,

based on the theoretical analysis. It illustrates that thiol **2** is an inert thiol with regard to catalysis. Furthermore, it illustrates that TEG-based monolayers do not have any affinity for the substrate. If nonspecific binding of HPNPP to TEG-monolayers had taken place, this would have resulted in an increase of the apparent K_M value (indicating weaker binding) upon lowering x_1 , since higher HPNPP concentrations would be required to saturate the catalyst.

Mixed monolayers composed of thiols 1 and 2 (series A): Analysis of the obtained k_{cat} values as a function of the mole fraction of **1** shows a nearly perfect linear increase up to $x_1=0.4$ and an intersect at origin when extrapolated to $x_1=0$ (Figure 5a:■). In our experimental set up, a mole fraction of $x_1=0$ corresponds to the dilution of a constant amount of **1** (20 μM) in an infinite amount of thiol **2**. In fact, the intersect close to 0 confirms that isolated TACN·Zn^{II} units surrounded by TEG have a negligible catalytic activity. The K_M values decrease exponentially as a function of the mole fraction x_1 (Figure 5b:■). From these observations, and taking into account the theoretical analysis, we can draw two conclusions for this mixed thiol system. First, clustering of thiol **1** does not appear to occur. In case of domain formation both parameters k_{cat} and K_M would have been practically constant already at very low x_1 values as confirmed by experiment series **B**. Rather, both the behavior of k_{cat} and K_M are fully compatible with the expected behavior for a random distribution of thiols. This is supported by the correspondence of the experimental data points representing the dependence of k_{cat} and K_M on x_1 with the simulated behavior for a random distribution of thiols (solid lines of Figure 5a and 5b). Importantly, independent proof for the statistical distribution of thiols **1** and **2** was very recently obtained from a study based on the quenching of anionic fluorescence probes bound to the Au MPC surface.^[58] The results of series **A** also leads towards the second conclusion. Although it appears on first sight that the catalytic sites on the surface change as a function of the mole fraction x_1 (increase k_{cat} ; decrease K_M), the theoretical analysis shows that this is an intrinsic behavior originating from the multivalency of the catalytic system. There is no reason to offer chemical explanations for these changes, which is similar to what we had observed for a related dendrimer study.^[42] Importantly, it shows the intrinsic advantage of using a multivalent scaffold.

Evaluation of catalytic SAMs on NPs: Previously, we have extensively studied a wide variety of transphosphorylation catalysts based on the same TACN·Zn^{II} catalytic unit (Figure 8). In all cases we have shown that catalysis requires the cooperative action of two catalytic units. For systems **3**^[42] and **4**,^[59] we were able to determine the Michaelis-Menten parameters, which are added in Table 2. By themselves these are reasonable catalysts in terms of rate acceleration (k_{cat}/k_{uncat}), but their activity becomes insignificant when compared to the NP-based system. The gain of the NP system lies mainly in a strongly increased k_{cat} value (>13

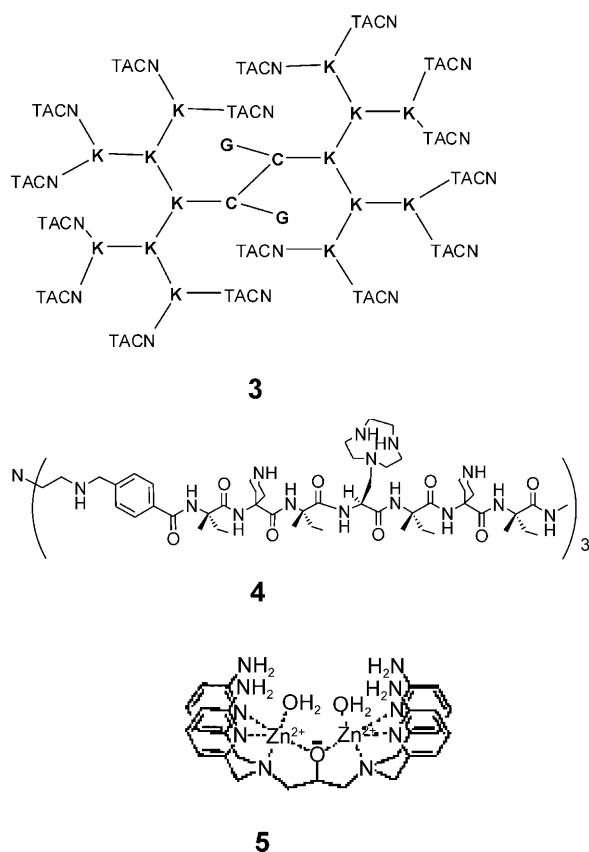


Figure 8. Structures of selected catalysts for the transesterification of HPNPP. The Michaelis–Menten parameters (corrected for the amount of Zn^{II} ions) are given in Table 2.

times compared to **3**) and to a lesser extent on an increased binding affinity (≈ 4 times compared to **3**). In a previous study,^[42] we had already discussed that lysine-based dendrimers are not optimal scaffolds for surface modifications, because of the asymmetric branching units. Nanoparticles are on the opposite side of the spectrum, inducing an excellent alignment of the catalytic units. It is worth considering that the best dimetallic catalysts known for the transphosphorylation of HPNPP are typically equipped with an alkoxy function in the spacer that coordinates to both metal centers and brings them in close proximity (for example **5**,^[52] Figure 8). This makes us postulate that the origin for the enhanced catalytic activity in the NPs is the close proximity of the Zn^{II} ions induced by the packing of the monolayer. In the monolayer all thiols are aligned and the head groups find themselves in close proximity with a relative low mobility. Apparently the spatial orientation of two neighboring catalytic units creates a perfect catalytic site without formation of catalytically inactive μ -hydroxo species.

Conclusion

We have studied the catalytic activity of a series of Au MPCs as a function of the catalyst loading on the surface.

Normalized for the number of metal centers, these systems are among the best catalysts known for the transphosphorylation of HPNPP exhibiting $k_{\text{cat}}/K_{\text{M}}$ values of more than $20 \text{ L mol}^{-1} \text{ s}^{-1}$. This is quite remarkable, considering the structural simplicity of the $\text{TACN} \cdot \text{Zn}^{\text{II}}$ catalytic unit. The fact that the same complex in other (multivalent) systems is much less active, indicates that the use of nanoparticles as scaffolds carries particular advantages. The reduced freedom of the complexes and the desolvation of the reacting nucleophile could be possible explanations,^[45,60] but the forced close packing of the $\text{TACN} \cdot \text{Zn}^{\text{II}}$ head groups is very likely to play an important role. The theoretical analysis showed the intrinsic advantage of the multivalent system in generating catalytic sites composed of two $\text{TACN} \cdot \text{Zn}^{\text{II}}$ complexes. The clustering of multiple catalytic units on the NP surface creates a large number of potential binding sites for the substrate, which increases as a function of the surface catalyst loading. Consequently, this gives the impression that the affinity of the substrate for the catalyst increases as the surface loading goes up (exponential decrease in K_{M}). Likewise, the apparent catalytic constant k_{cat} is smaller for low catalyst loadings, because individual residues cannot participate in the formation of catalytic sites resulting in a lower activity at saturation. Our experimental data indicate an increase in the apparent k_{cat} up till a molar fraction of ≈ 0.4 after which it remains practically constant. The apparent K_{M} value on the other hand shows an exponential decay as a function of the surface loading. The result is a continuous increase in $k_{\text{cat}}/K_{\text{M}}$ as a function of the catalyst loading. Without the theoretical analysis, this would have been ascribed to an improvement in the catalytic site or to other reasons of chemical origin. However, the profiles perfectly match those that are intrinsic to the multivalent system, which implies that the catalytic site is more or less the same over the range of mole fractions studied. The experimentally observed trends for k_{cat} and K_{M} also suggest that the two thiols (**1** and **2**) are more or less randomly distributed on the NP surface. Clustering would have resulted in nearly constant values for these parameters over the whole range studied or, as a minimum, would have resulted in a much faster arrival at a constant k_{cat} value (before $x_1 \approx 0.2$). This was confirmed experimentally by performing a mixing experiment in which the catalytic activity of different ratios of homofunctionalized nanoparticles was measured. This observation is different from that observed for other systems,^[30] but surface ordering is presumably strongly dependent on the chemical nature of the thiols.

In summary, this first detailed investigation of catalytic SAMs has given new insights on the intrinsic catalytic behavior that can be expected for these multivalent systems. It clearly evidences that experimental data on catalysis should be analysed properly, before claiming a real “dendritic” effect, that is, an increase of the efficiency of the catalyst with its valency. Additionally, it has allowed us to indirectly obtain information on the structural order within the SAM. Based on these studies we now intend to develop a second generation of catalysts in which the bystander thiol will

tailor the properties of the catalytic units. Eventually, this should lead to truly engineered catalytic nanoarchitectures.

Experimental Section

NMR spectra were recorded on a Bruker Avance 300 MHz spectrometer operating at 301 K. UV/Vis spectra were recorded on a Perkin-Elmer Lambda 16 spectrophotometer equipped with a thermostatted cell holder. The kinetic measurements were performed on a TECAN-Infinite F200 microplate reader equipped with a 405(±10) nm using Greiner transparent flat-bottom 96-well plates. TEM images were recorded on a Jeol 300 PX electron microscope. The synthesis of compounds **1**^[32] and **2**^[39] has been reported previously.

Nanoparticle synthesis: HAuCl₄·3 H₂O (102 mg, 0.26 mmol), weighed in a dry-box, was dissolved in H₂O (mQ; 7 mL). Separately, a solution of TOABr (5.50 g, 3 mmol) in degassed toluene (250 mL) was prepared. The aqueous solution of Au^{III} was extracted with the TOABr-solution (3×15 mL) causing a transfer of the gold ions to the organic phase (red color). Di-*n*-octylamine (4.3 mL, 14 mmol) was then added to the remaining amount of the TOABr solution, and the resulting mixture was vigorously stirred with the Au^{III}-containing solution for 30 min under N₂ resulting in a complete decoloration of the solution. Subsequently, NaBH₄ (46 mg, 1.2 mmol) dissolved in H₂O (2 mL) was added under vigorous stirring resulting in the formation of the Au nanoparticles (brown coloring). The solution was stirred for an additional 3 h under N₂, after which the aqueous phase was removed. The resulting nanoparticle solution was stored under an inert atmosphere over night. The nanoparticle solution was divided in eight batches and thiols **1** and **2** were added in different ratios from stock solutions in DMF. The two thiols were mixed before being added to the nanoparticles under vigorous stirring. Within 15 min the solution became colorless and a brown precipitate was formed. After 5 min H₂O (mQ; 5 mL) was added and the solution was stirred for an hour under N₂. Next, the aqueous phase was separated and washed with diethyl ether (2×10 mL), toluene (4×10 mL), ethylacetate (3×10 mL), and again diethyl ether (2×10 mL). Finally, water was removed by evaporation under reduced pressure and the Au MPCs were obtained as brown solids.

Spectrophotometric titrations with Cu^{II}: Two cuvettes were prepared containing a 0.1 M solution of MES (80 μL) at pH 6.5, the stock solution of nanoparticles (48 μL) with unknown concentration and H₂O (mQ; 672 μL). The titrating solution contained CuCl₂ (0.6 mM) and MES (10 mM) in H₂O (mQ). An additional solution containing only MES (10 mM) in H₂O (mQ) was used to correct for the dilution of the reference cuvette. The absorbance was measured at 264 nm after adding the Cu^{II}-containing solution to one cuvette and the buffer solution to the reference cuvette.

Kinetic measurements: Kinetics were measured at 40 °C in aqueous solution, buffered at pH 7.5 with HEPES 0.01 M. Reaction mixtures were prepared by adding in order the solution of nanoparticles, a solution of Zn(NO₃)₂, and a solution of HPNPP in water. The cleavage of the phosphodiester was monitored by measuring the absorbance of *p*-nitrophenolate at 405 nm. Initial velocities were calculated by a linear fitting of the initial part of the kinetics (conversion < 10%).

Acknowledgements

Financial support from the European Research Council under the European Community's Seventh Framework Programme (FP7/2007-2013)/ERC Starting Grant agreement n° 239898 is acknowledged.

[1] R. A. Sheldon, I. Arends, U. Hanefeld, *Green Chemistry and Catalysis*, 1st ed., Wiley-VCH, Weinheim, 2007.

- [2] A. Thomas, M. Driess, *Angew. Chem.* **2009**, *121*, 1922–1924; *Angew. Chem. Int. Ed.* **2009**, *48*, 1890–1892.
- [3] F. M. de Rege, D. K. Morita, K. C. Ott, W. Tumas, R. D. Broene, *Chem. Commun.* **2000**, 1797–1798.
- [4] C. Bianchini, P. Barbaro, V. Dal Santo, R. Gobetto, A. Meli, W. Oberhauser, R. Psaro, F. Vizza, *Adv. Synth. Catal.* **2001**, *343*, 41–45.
- [5] R. Margalef-Català, C. Claver, P. Salagre, E. Fernández, *Tetrahedron: Asymmetry* **2000**, *11*, 1469–1476.
- [6] M. J. Alcón, A. Corma, M. Iglesias, F. Sánchez, *J. Mol. Catal. A* **1999**, *144*, 337–346.
- [7] P. Barbaro, F. Liguori, *Chem. Rev.* **2009**, *109*, 515–529.
- [8] I. Yosef, R. Abu-Reziq, D. Avnir, *J. Am. Chem. Soc.* **2008**, *130*, 11880–11882.
- [9] M. Bartz, J. Kuther, R. Seshadri, W. Tremel, *Angew. Chem.* **1998**, *110*, 2646–2649; *Angew. Chem. Int. Ed.* **1998**, *37*, 2466–2468.
- [10] M. C. Daniel, D. Astruc, *Chem. Rev.* **2004**, *104*, 293–346.
- [11] S. Roy, M. A. Pericas, *Org. Biomol. Chem.* **2009**, *7*, 2669–2677.
- [12] T. Belsler, M. Stohr, A. Pfaltz, *J. Am. Chem. Soc.* **2005**, *127*, 8720–8731.
- [13] H. M. R. Gardimalla, D. Mandal, P. D. Stevens, M. Yen, Y. Gao, *Chem. Commun.* **2005**, 4432–4434.
- [14] A. G. Hu, G. T. Yee, W. B. Lin, *J. Am. Chem. Soc.* **2005**, *127*, 12486–12487.
- [15] F. Manea, F. B. Houillon, L. Pasquato, P. Scrimin, *Angew. Chem.* **2004**, *116*, 6291–6295; *Angew. Chem. Int. Ed.* **2004**, *43*, 6165–6169.
- [16] P. Pengo, S. Polizzi, L. Pasquato, P. Scrimin, *J. Am. Chem. Soc.* **2005**, *127*, 1616–1617.
- [17] R. Bonomi, F. Selvestrel, V. Lombardo, C. Sissi, S. Polizzi, F. Mancin, U. Tonellato, P. Scrimin, *J. Am. Chem. Soc.* **2008**, *130*, 15744.
- [18] T. Belsler, E. N. Jacobsen, *Adv. Synth. Catal.* **2008**, *350*, 967–971.
- [19] P. Scrimin, G. Ghirlanda, P. Tecilla, R. A. Moss, *Langmuir* **1996**, *12*, 6235–6241.
- [20] P. Scrimin, P. Tecilla, U. Tonellato, C. A. Bunton, *Colloids Surfaces A* **1998**, *144*, 71–79.
- [21] C. A. Bunton, P. Scrimin, P. Tecilla, *J. Chem. Soc. Perkin Trans. 2* **1996**, 419–425.
- [22] J. M. J. Frechet, *Science* **1994**, *263*, 1710–1715.
- [23] L. Ropartz, R. E. Morris, D. F. Foster, D. J. Cole-Hamilton, *Chem. Commun.* **2001**, 361–362.
- [24] A. Dahan, M. Portnoy, *Org. Lett.* **2003**, *5*, 1197–1200.
- [25] Y. Ribourdouille, G. D. Engel, M. Richard-Plouet, L. H. Gade, *Chem. Commun.* **2003**, 1228–1229.
- [26] E. Delort, T. Darbre, J. L. Reymond, *J. Am. Chem. Soc.* **2004**, *126*, 15642–15643.
- [27] C. C. Paluti, E. S. Gawalt, *J. Catal.* **2009**, *267*, 105–113.
- [28] A. M. Jackson, J. W. Myerson, F. Stellacci, *Nat. Mater.* **2004**, *3*, 330–336.
- [29] L. Duchesne, G. Wells, D. G. Fernig, S. A. Harris, R. Levy, *Chem-BioChem* **2008**, *9*, 2127–2134.
- [30] C. Gentilini, P. Franchi, E. Mileo, S. Polizzi, M. Lucarini, L. Pasquato, *Angew. Chem.* **2009**, *121*, 3106–3110; *Angew. Chem. Int. Ed.* **2009**, *48*, 3060–3064.
- [31] C. Gentilini, L. Pasquato, *J. Mater. Chem.* **2010**, *20*, 1403–1412.
- [32] F. Manea, C. Bindoli, S. Polizzi, L. Lay, P. Scrimin, *Langmuir* **2008**, *24*, 4120–4124.
- [33] N. R. Jana, X. G. Peng, *J. Am. Chem. Soc.* **2003**, *125*, 14280–14281.
- [34] A. C. Templeton, M. J. Hostetler, E. K. Warmoth, S. W. Chen, C. M. Hartshorn, V. M. Krishnamurthy, M. D. E. Forbes, R. W. Murray, *J. Am. Chem. Soc.* **1998**, *120*, 4845–4849.
- [35] M. J. Hostetler, A. C. Templeton, R. W. Murray, *Langmuir* **1999**, *15*, 3782–3789.
- [36] L. Pasquato, F. Rancan, P. Scrimin, F. Mancin, C. Frigeri, *Chem. Commun.* **2000**, 2253–2254.
- [37] R. Shenhar, V. M. Rotello, *Acc. Chem. Res.* **2003**, *36*, 549–561.
- [38] R. Klajn, K. J. M. Bishop, B. A. Grzybowski, *Proc. Natl. Acad. Sci. USA* **2007**, *104*, 10305–10309.
- [39] P. Pengo, S. Polizzi, M. Battagliarin, L. Pasquato, P. Scrimin, *J. Mater. Chem.* **2003**, *13*, 2471–2478.

- [40] A. Scarso, G. Zaupa, F. B. Houillon, L. J. Prins, P. Scrimin, *J. Org. Chem.* **2007**, *72*, 376–385.
- [41] M. Martin, F. Manca, R. Fiammengo, L. J. Prins, L. Pasquato, P. Scrimin, *J. Am. Chem. Soc.* **2007**, *129*, 6982–6983.
- [42] G. Zaupa, P. Scrimin, L. J. Prins, *J. Am. Chem. Soc.* **2008**, *130*, 5699–5709.
- [43] G. Zaupa, L. J. Prins, P. Scrimin, *Bioorg. Med. Chem. Lett.* **2009**, *19*, 3816–3820.
- [44] T. Darbre, J. L. Reymond, *Acc. Chem. Res.* **2006**, *39*, 925–934.
- [45] P. Pengo, L. Baltzer, L. Pasquato, P. Scrimin, *Angew. Chem.* **2007**, *119*, 404–408; *Angew. Chem. Int. Ed.* **2007**, *46*, 400–404.
- [46] R. Breinbauer, E. N. Jacobsen, *Angew. Chem.* **2000**, *112*, 3750–3753; *Angew. Chem. Int. Ed.* **2000**, *39*, 3604–3607.
- [47] D. H. Wu, A. D. Chen, C. S. Johnson, *J. Magn. Reson. Ser. A* **1995**, *115*, 260–264.
- [48] The use of large gradient pulses in diffusion-ordered 2D NMR spectroscopy (DOSY) results in the induction of eddy currents in the metal structures of the magnet and probe, which causes a distortion in the high-resolution spectra. The LEDbp sequence reduces that problem by using bipolar pulse pairs, since the eddy currents caused by two gradient pulses with identical areas, but different polarities tend to cancel.
- [49] D. M. Brown, D. A. Usher, *J. Chem. Soc.* **1965**, 6558–6564.
- [50] It should be noted that the initial rate obtained for $[Zn^{II}] = 0$ is an experimental point.
- [51] Under the experimental conditions thiol exchange between the nanoparticle is much slower than the kinetic process studied; see: M. Zachary, V. Chechik, *Angew. Chem.* **2007**, *119*, 3368–3371; *Angew. Chem. Int. Ed.* **2007**, *46*, 3304–3307.
- [52] G. Q. Feng, D. Natale, R. Prabakaran, J. C. Mareque-Rivas, N. H. Williams, *Angew. Chem.* **2006**, *118*, 7214–7217; *Angew. Chem. Int. Ed.* **2006**, *45*, 7056–7059.
- [53] F. Avenier, J. B. Domingos, L. D. Van Vliet, F. Hollfelder, *J. Am. Chem. Soc.* **2007**, *129*, 7611–7619.
- [54] F. Mancin, P. Scrimin, P. Tecilla, U. Tonellato, *Chem. Commun.* **2005**, 2540–2548.
- [55] Simulations using a dodecahedron (12 faces) or icosahedron (20 faces) gave essentially identical results (data not shown). This indicates that, at least from a theoretical point of view, the polydispersity of the nanoparticles is less relevant. This originates from the fact that the catalytic site is composed of only 12 units, which is far less than the total number of thiols present in the monolayer. Experimentally, polydispersity may cause a different spacing between two catalytic units, resulting in different efficiency. However, the similarity of the catalytic parameters of the nanoparticles presented here (1.6 ± 0.2 nm) and those of a previous study (2.5 ± 0.7 nm, ref. [15]) indicate that polydispersity does not appear to play an important role. For that reason, and also considering the relative narrow size distribution of the nanoparticles here, polydispersity was not taken into account in the analysis.
- [56] S. L. Regen, *Curr. Opin. Chem. Biol.* **2002**, *6*, 729–735.
- [57] S. M. K. Davidson, S. L. Regen, *Chem. Rev.* **1997**, *97*, 1269–1279.
- [58] R. Bonomi, A. Cazzolaro, L. J. Prins, *Chem. Commun.* **2011**, *47*, 445–447.
- [59] A. Scarso, U. Scheffer, M. Gobel, Q. B. Broxterman, B. Kaptein, F. Formaggio, C. Toniolo, P. Scrimin, *Proc. Natl. Acad. Sci. USA* **2002**, *99*, 5144–5149.
- [60] F. Avenier, F. Hollfelder, *Chem. Eur. J.* **2009**, *15*, 12371–12380.

Received: September 7, 2010

Revised: November 22, 2010

Published online: March 14, 2011